Sustainable Cities and Society 116 (2024) 105912

Contents lists available at ScienceDirect

Sustainable Cities and Society

journal homepage: www.elsevier.com/locate/scs

Study on the spatiotemporal pattern evolution of surface urban heat island in shrinking cities: Fushun and Tieling

Yanfei Wu [a], Junjie Qiu [a], Jiake Wang [a], Wenyuan Wu [a,b], Ting Wu [a], Hao Hou [a,b], Haiping Xia [a,b], Junfeng Xu [a,b,*]

[a] Institute of Remote Sensing and Earth Sciences, Hangzhou Normal University, Yuhangtang Road No 2318, Hangzhou 311121, PR China
[b] Zhejiang Provincial Key Laboratory of Urban Wetlands and Regional Change, Hangzhou, 311121, PR China

ARTICLE INFO

Keywords:
Shrinking cities
Surface urban heat island
Spatiotemporal evolution
Landscape metrics

ABSTRACT

Under rapid urbanization, the urban heat island (UHI) problem impacts not only large cities, but also poses severe challenges to shrinking cities with rapidly declining population. In China, most shrinking cities are characterized by population loss alongside the expansion of built-up areas due to policy. Urban warming exacerbates the human settlement environment, with UHI intensifying due to urban expansion, while population loss simultaneously alleviates it. This raises a question: will the UHI problem be mitigated in shrinking cities? In this study, we analyze the spatiotemporal pattern evolution of surface urban heat island (SUHI) in Fushun and Tieling from 2000 to 2020 using Landsat series products. We combine landscape pattern indices and SUHI indicators, and perform correlation analyses of the factors influencing SUHI with multiscale geographically weighted regression (MGWR). The findings reveal that in Fushun, mining activities significantly impact SUHI, while in Tieling, extremely Land Surface Temperature (LST) zones are expanding and dispersing. SUHI patterns are notably shaped by subsurface conditions, and spatial configurations play key roles in regulating SUHI. However, population loss has not significantly influenced SUHI, even in shrinking cities. This study offers a new perspective for SUHI research and provides further insights into urban planning strategies.

1. Introduction

Since the 21st century, rapid urbanization has driven significant economic development (L. Li et al., 2023), but also profoundly affected the urban ecological environment (Li et al., 2023b), leading to numerous environmental issues (Cheng et al., 2023; Ding & Liu, 2023), including the UHI phenomenon (Ellena et al., 2023), which has drawn widespread concerns (D. Han et al., 2023; Zhang et al., 2022). Based on urban atmosphere layers, UHI can be categorized into four types, including SUHI and Canopy Urban Heat Island (CUHI) (Oke, 1995; Voogt & Oke, 2003). CUHI focuses on canopy level air temperature, using data from meteorological stations or traversed vehicles (Li et al., 2023c), with data collection limited. However, SUHI studies rely on LST from thermal infrared sensors (Weng et al., 2004), which are more accessible. Studies have also shown that CUHI and SUHI exhibit daytime similarities (Peng, 2022; J. Wang et al., 2023), thus, SUHI is now commonly used in research. Numerous scholars have investigated SUHI (Jibitha et al., 2024; Reed & Sun, 2023; Zhu et al., 2022), finding significant positive correlations between SUHI changes and factors like population growth and urban expansion in various regions (Mohammad & Goswami, 2023; J. Wang et al., 2023). Research also indicates that in large, dense cities, higher levels of anthropogenic heat release increase urban "skin" temperature as the population grows (Manoli et al., 2019). However, other studies suggest that population changes do not always influence SUHI

Abbreviation: **UHI**, Urban Heat Island; **SUHI**, Surface Urban Heat Island; **MGWR**, Multiscale Geographically Weighted Regression; **LST**, Land Surface Temperature; **CUHI**, Canopy Urban Heat Island; **USGS**, United States Geological Survey; **GEE**, Google Earth Engine; **NASA**, National Aeronautics and Space Administration; **SRTM**, Shuttle Radar Topography Mission; **LEDAPS**, Landsat Ecosystem Distribution Adaptive Processing System; **LaSRC**, Land Surface Reflectance Code; **CF Mask**, C Function of Mask; **PLAND**, Percentage of Landscape; **PD**, Patch Density; **LPI**, Largest Patch Index; **LSI**, Landscape Shape Index; **AI**, Aggregation Index; **CONTAG**, Contagion index; **SHDI**, Shannon's Diversity Index; **RF**, Random Forest; **GIS**, Geographic Information System; **IS**, Impervious Surface; **MSU**, Mean Surface Urban Heat Island Index; **SUR**, Surface Urban Heat Island Index Ratio; **SUSD**, Surface Urban Heat Island Index Standard Deviation; **AICc**, corrected Akaike Information Criterion; **NDVI**, Normalized Difference Vegetation Index; **BSI**, Bare Soil Index.

* Corresponding author at: Institute of Remote Sensing and Earth Sciences, College of Science, Hangzhou Normal University, Hangzhou, 311121, PR China.
E-mail address: 20090019@hznu.edu.cn (J. Xu).

https://doi.org/10.1016/j.scs.2024.105912
Received 7 June 2024; Received in revised form 14 October 2024; Accepted 15 October 2024
Available online 19 October 2024

(Pena Acosta et al., 2023; Wang et al., 2023d). Since most research has focused on cities with population growth and urban expansion, the specific impacts of population remain challenging to analyze. Therefore, studying shrinking cities with declining populations could offer a new insight into SUHI research (Liu & Zhang, 2024).

A shrinking city is one that experiences a sustained population decrease over a specific period (Khavarian-Garmsir, 2023). Due to the combined effects of globalization, deindustrialization, suburbanization, and population aging, nearly a quarter of the world's cities are facing various degrees of population shrinkage (Wu & Yao, 2021). This trend poses significant challenges to urban economic development, leading to issues such as reduced social vitality (Zeng et al., 2022), stagnant economic growth (Lee et al., 2023), and an increase in vacant properties (Jang & Kim, 2021). However, population decline can also ease ecological pressures, providing opportunities to enhance the urban environment (D. Chen et al., 2023). Additionally, population loss reduces various forms of anthropogenic heat (Peng et al., 2022), which helps to mitigate the SUHI problem to some extent (Mansour et al., 2022; Jin et al., 2020).

It is widely recognized that the key factors influencing SUHI are land cover changes, anthropogenic activities, and others (Jabbar et al., 2023). Urban development-driven land use changes alter surface properties, with impervious surfaces showing significantly higher LST than rural areas, further intensifying the UHI effect (Chen et al., 2023b; Ma et al., 2023). Moreover, the geometric configuration of urban buildings affects wind flow, energy absorption and emission, which has driven studies in the three-dimensional aspects (Han et al., 2023b; Shao et al., 2023). Heat generated by anthropogenic activities, including industry, transportation, construction, and daily human activities, is often represented by population parameters in studies (Moazzam & Lee, 2024; Pan et al., 2024), as larger population typically leads to higher energy consumption. In addition, weather conditions and geographic location affect SUHI, though these factors are largely beyond the control of local communities (Sima et al., 2024), and thus require careful consideration in research.

Although many studies have been conducted, there are still differing views on whether population factors influence SUHI (Cai et al., 2021; Liu & Zhang, 2024). While most researches focus on the macro level (Peng et al., 2022), the specific spatiotemporal pattern of SUHI within shrinking cities remains underexplored. Unlike conventional shrinking cities, population decline in China's shrinking cities occurs alongside spatial expansion (Sun & Zhou, 2022). This reality, however, has been overlooked by Chinese planners and local authorities who pursue urbanization (Meng & Long, 2022), leading to an oversupply in built environment of these cities (Long & Gao, 2019). The coexistence of population loss and spatial expansion in Chinese shrinking cities makes the spatial pattern of SUHI and the factors influencing it more distinct. This analysis provides theoretical support for developing targeted management strategies to mitigate and ultimately alleviate the SUHI problem (Lin et al., 2024).

Therefore, this study utilizes Landsat satellite data to analyze the spatiotemporal patterns of SUHI in Fushun and Tieling, two different types of shrinking cities, from 2000 to 2020. The main objective is to investigate how SUHI patterns change in response to population loss and spatial expansion, and to identify the factors influencing these changes. The paper focus on three key aspects: (1) Refining the specific spatiotemporal pattern evolution of SUHI in shrinking cities; (2) Exploring the impacts of population loss and spatial expansion on these cities; and (3) Comparing the SUHI pattern in Fushun and Tieling. Through this study, we aim to enhance the understanding of SUHI and its spatiotemporal characteristics in shrinking cities, verify the impact of population on SUHI, and analyze the factors affecting it, ultimately contributing to solutions for the SUHI problem.

2. Materials and methods

2.1. Study area

Fushun (123°40′ - 125°29′ E and 41°14′ - 42°29′ N) and Tieling (123°27′ - 125°06′ E and 41°59′ - 43°29′ N) are located in northeastern Liaoning Province, China, near the provincial capital, Shenyang. Fushun's terrain features higher elevations in the north and south, with a lower central valley where the Hun River flows east to west, and the built-up areas are primarily concentrated in this valley. Tieling's terrain has higher elevations in the southeast and lower ones in the northwest, extending into the Liao River Plain and hilly terrain. Its built-up areas are mainly situated on the plains. Both cities experience a temperate continental monsoon climate, characterized by cold, dry winters, warm, rainy summers, and ample sunshine (LPBS, 2020).

Both Fushun and Tieling are experiencing continuous population decline, fitting the definition of shrinking cities (Sun et al., 2024; Xu & Zhang, 2024). Fushun is a typical coal resource-dependent shrinking city. For decades, the coal industry dominated Fushun, with numerous mining areas scattered throughout the city (Wei et al., 2023). However, the closure and development of mining areas, along with their ecological restoration, declining labor demand, and population outflow due to industrial upgrading (Zhang, 2022), may all impact the spatiotemporal pattern of SUHI. Unlike Fushun, Tieling does not have a dominant industrial sector, but has faced a steady population decline for many years due to various factors (Yu et al., 2023).

The study areas were selected based on the research by Yang et al., choosing approximately half of the city's equivalent diameter, as this range had the most significant impact on UHI mitigation (Yang et al., 2024). The urban areas were extracted using class 13 from the Land Cover Type 1 of the MODIS MCD12Q1 product (Fig. 1).

2.2. Data pre-processing and overall workflow

This study utilized Landsat series data for LST retrieval and feature classification, sourced from the official USGS (United States Geological Survey, http://earthexplorer.usgs.gov/) website. We conducted the LST retrieval process on the Google Earth Engine (GEE) platform. Since SUHI is significant in summer, the selected data consisted of images from June to August with cloud cover below 10 % (Chauhan & Singh Jethoo, 2023), ensuring high image quality. Additionally, to eliminate the influence of terrain factors, we applied terrain correction in the GEE code using National Aeronautics and Space Administration (NASA)'s Shuttle Radar Topography Mission (SRTM) Digital Elevation data. The land cover classification data were sourced from secondary products provided by the USGS, the specific image data used are provided in Table 1.

The population data used in the study were obtained from the Landscan population raster dataset, published by Oak Ridge National Laboratory (https://landscan.ornl.gov/). Known for its reliability and accuracy, this dataset has been widely employed in various studies, involving population data (Yagoub et al., 2024; Aslam et al., 2023). With a spatial resolution of 1 km, the dataset was reprojected to match the projection type of the study area.

The study selected Landscan population dataset to represent population decline and landscape pattern indices to represent spatial expansion, both key factors influencing SUHI and widely used in previous research (Guan et al., 2023; Shen et al., 2023; Wu et al., 2022). These factors also reflect the main influences of land cover changes and anthropogenic activities on SUHI. Given the minimal elevation differences in the study area, terrain was excluded, while MGWR analysis was used to account for location factors by incorporating latitude and longitude data.

The overall workflow of the study is shown in Fig. 2.

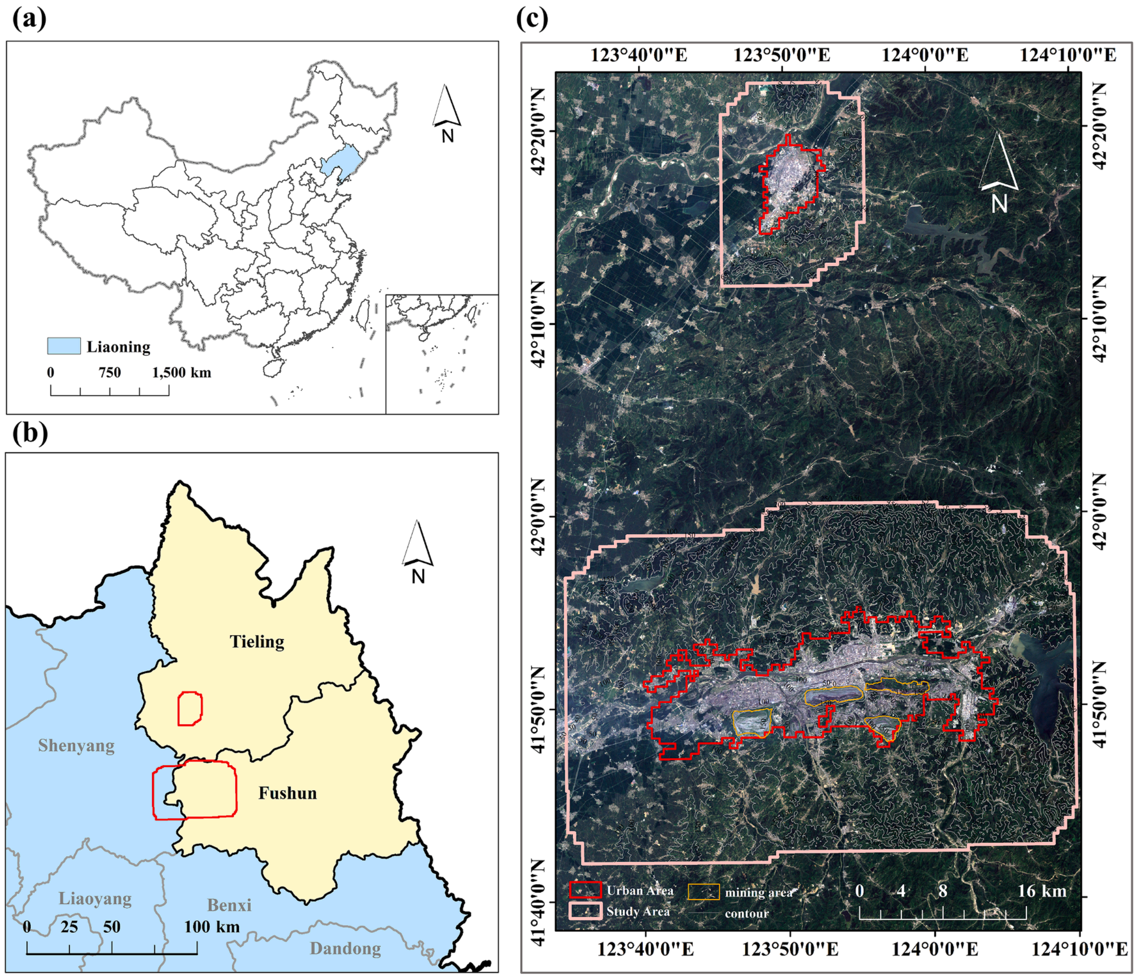

Fig. 1. Map of the study area: (a) Map of China; (b) Map of Liaoning; (c) Landsat-5 image of the study area displayed in true color composite.

Table 1
Descriptions of the Landsat images used for land cover classification.

City	Year	Sensor	Acquisition date and time (local time)
Fushun	2000	Landsat-5 TM	31 July 2000 (10:05:35)
	2007	Landsat-5 TM	19 July 2007 (10:22:02)
	2014	Landsat-8 OLI/TIRS	9 August 2014 (10:28:09)
	2020	Landsat-8 OLI/TIRS	22 July 2020 (10:28:18)
Tieling	2000	Landsat-5 TM	31 July 2000 (10:05:35)
	2006	Landsat-5 TM	17 August 2006 (10:21:37)
	2014	Landsat-8 OLI/TIRS	7 August 2014 (10:28:25)
	2020	Landsat-8 OLI/TIRS	22 July 2020 (10:28:18)

2.3. *Retrieval of land surface temperature (LST) and surface urban heat island (SUHI) intensity*

GEE developers have preprocessed the Landsat series satellite images, including applying the Landsat Ecosystem Distribution Adaptive Processing System (LEDAPS) and the Land Surface Reflectance Code (LaSRC) algorithms for atmospheric correction. Then, the C Function of Mask (CF Mask) is used to identify cloud, shadow, water and snow mask for each pixel (Najafzadeh et al., 2021). To avoid interference from extreme weather, we selected images with <10 % cloud cover from June to August for LST synthesis. We then used the CF Mask algorithm to remove low-quality pixels.

The study employed ΔLST to quantify the SUHI effect (Jallu et al., 2022; Wang et al., 2023b). In this study, ΔLST was defined as the difference between each pixel value and the average value across the entire suburban area of the city, calculated using the following formula:

$$\Delta LST = LST_{Pixel} - LST_{Suburban} \tag{1}$$

where LST_{Pixel} represents the LST value of each pixel in the LST map. $LST_{Suburban}$ is the mean LST over other non-urban areas and water pixels (Zeng et al., 2023).

To further analyze the spatiotemporal pattern of thermal, the study also employed another widely used classification method, based on hierarchical classification of LST (Yue et al., 2024; Shen et al., 2023). This method utilized the LST data obtained from GEE and applied the mean-standard deviation approach to classify each image into eight categories. The specific classification criteria are detailed in Table 2.

2.4. *Surface urban heat island (SUHI) indicators*

To more effectively depict the spatial pattern of SUHI, this study also employed several simple indicators: mean SUHI (MSU), SUHI ratio (SUR), and SUHI standard deviation (SUSD). These indicators offered a clearer understanding of SUHI patterns and characterization. The SUR was designed based on the MSU of the study area, with approximately 30 % of ΔLST values exceeding 2 °C in both study areas. The specific calculation formulas are shown in Table 3.

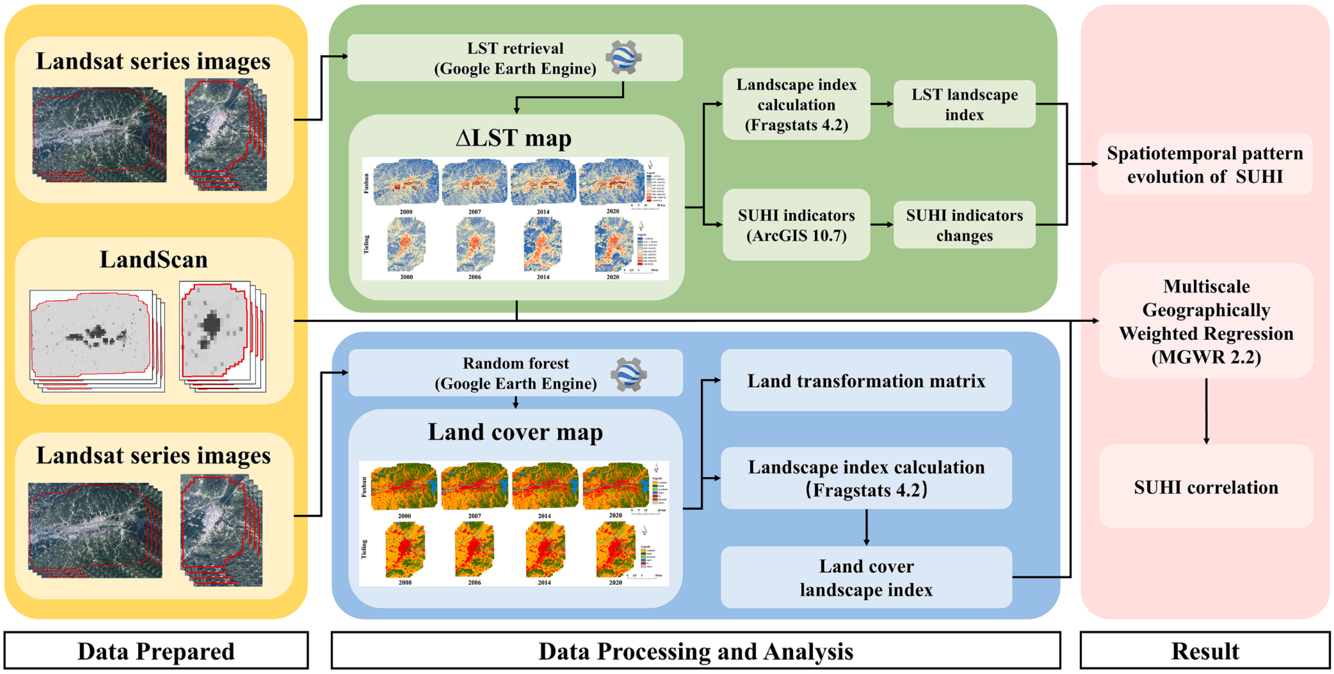

Fig. 2. Workflow of the study.

Table 2
Land surface temperature classifications.

Level	Type	Division Standard
1	Extremely low	$T < \mu$ - 1.5std
2	Very low	μ - 1.5std $\leq T < \mu$ - std
3	Low	μ - std $\leq T < \mu$ - 0.5std
4	Medium low	μ - 0.5std $\leq T < \mu$
5	Medium high	$\mu \leq T \leq \mu$ + 0.5std
6	High	μ + 0.5std $< T \leq \mu$ + std
7	Very high	μ + std $< T \leq \mu$ + 1.5std
8	Extremely high	$T > \mu$ + 1.5std

Table 3
Discription of SUHI indicators in the study.

SUHI indicators	Formula	Descriptions
mean SUHI (MSU)	$MSU = \frac{\sum_{i=1}^{n} N_i}{n}$	Mean ΔLST in the study area.
SUHI ratio (SUR)	$SUR = \frac{N_s}{n}$	The proportion of ΔLST higher than 2 °C.
SUHI standard deviation (SUSD)	$SUSD = \sqrt{\frac{\sum_{i=1}^{n} (N_i - N_{mean})^2}{n}}$	Variation degree of the ΔLST in the study area.

Note: N_i is the ΔLST of each pixel; n is the number of pixels in the analyst unit; N_s is the pixel numbers of ΔLST values higher than 2 °C; N_{mean} is the mean ΔLST of all pixels.

2.5. Landscape pattern index

The composition and configuration of a city's landscape significantly influence the distribution of LST and SUHI (Shao et al., 2023). These factors are often quantified using landscape pattern indices to further analyze urban landscapes (Ke et al., 2021; Karunaratne et al., 2022; Chen et al., 2023c). In this study, we synthesized previous research and selected seven indices that effectively reflect the landscape pattern: percentage of landscape (PLAND), patch density (PD), largest patch index (LPI), landscape shape index (LSI), aggregation index (AI), contagion index (CONTAG), and Shannon's diversity index (SHDI). The first five indices are under class metrics, useful for analyzing the patterns of different features. CONTAG and SHDI are landscape metrics, which access the overall landscape pattern of the entire study area. The specific meanings of each index are detailed in **Tab. A.1**.

To examine similarities and variations in landscape patterns across different scales, we established four study scales: 300 m, 600 m,900 m, and 1200 m, based on previous studies (Han et al., 2023b; Wu et al., 2022). Subsequently, we investigated the key factors influencing SUHI at each scale.

2.6. Land cover classification

The Random Forest (RF) model is widely employed in land cover classification owing to its high accuracy, non-parametric nature, and ability to determine variable importance (Rodriguez-Galiano et al., 2012). The GEE platform enhances the processing and analysis of vast satellite data. Using GEE with remote sensing, Geographic Information System (GIS) technology, and machine learning classifiers allows for the rapid and accurate creation of spatial maps that depict land use, land cover, and other earth surface features (M et al., 2023).

In this study, we utilized the RF model on the GEE platform to classify features into seven categories: impervious surface (IS), forest, cropland, grassland, water, bare land and others. We did not classify bare land due to the limited number of pixels in Tieling. Specific image data are detailed in Table 1. The final model achieved an overall accuracy of over 90 % and a kappa coefficient exceeding 85 %. To verify the mapping accuracy, we generated 500 random points in Fushun and 300 in Tieling for each year (Cuypers et al., 2023; Dash et al., 2023). And we used Google historical images with dates similar to the Landsat images as reference data (Han et al., 2023b).

2.7. Multiscale geographically weighted regression (MGWR)

The MGWR method distinguishes between local and global scale processes for various covariate effects, offering significant advantages over traditional regression methods in modeling spatial processes that closely resemble real-world scenarios (Yu et al., 2020). In this study, landscape pattern indices and population were computed as independent variable, with ΔLST serving as the dependent variable. The analysis was conducted using MGWR 2.2 software developed by Oshan (Oshan et al., 2019). The selection criteria for kernel function and bandwidth were based on the commonly used quadratic kernel function and the corrected Akaike Information Criterion (AICc), as shown in the following equations:

$$y_i = \sum_{j=1}^{k} \beta_{b_{wj}}(ui, vi)x_{ij} + \varepsilon \tag{2}$$

where y_i is the response variable, x_{ij} is the covariate, $\beta_{b_{wj}}$ is the j-th local regression coefficient with bandwidth b_w, (ui, vi) is the spatial geographic location of the point, and ε is the residual of the model regression.

The MGWR2.2 software independently computed and compared the results of GWR and MWGR. In this study, MGWR outperformed GWR in terms of both AICc and R^2. Therefore, the superior performance of MGWR was used directly in subsequent model selection and the presentation of results.

3. Results

3.1. Spatiotemporal pattern evolution of surface urban heat island (SUHI)

Fig. 3 illustrates the ΔLST maps for Fushun and Tieling from 2000 to 2020. In Fushun, high SUHI areas were primarily concentrated in the central urban region and mining areas. Over time, the central urban LST expanded outward, while high LST in mining regions shifted with changes in mining activity. In 2000, three key areas exhibited high LST: the West Dumping Site (Fig. 3 Fushun part 1), the East Dumping Site (Fig. 3 Fushun part 3), and the West Open-Pit (Fig. 3 Fushun part 4). By 2007, LST in the West Dumping Site began to decline, while it increased in the eastern and northern urban areas. By 2014, LST in the West Dumping Site had dissipated, but it rose in the East Open-Pit (Fig. 3 Fushun part 2). By 2020, high LST area was mainly located in the western urban area south of the river, the central urban area, the East Open-Pit, the West Open-Pit, and the urban area north of the river.

In Tieling, a single high SUHI area was present in the city center in 2000. By 2006, LST had increased and was expanding outward. By 2014, LST had spread significant, with several smaller high LST areas emerging in the south. By 2020, its extent continued to expand, with new high LST areas appearing in the northeast, indicating a general trend of SUHI dispersion.

The study categorized LST into eight levels using the grading method described in Section 2.3. To provide a more detailed quantification of the eight LST levels, landscape pattern indices were computed for each level, including PLAND, LPI, LSI, AI, CONTAG, and SHDI. Year-to-year changes in these indices were then calculated, with positive slopes indicating increases and negative slopes indicating decreases. The results of these slopes are presented in Table 4.

In Fushun, the total areas of the extremely low, very low, medium low and high LST zones increased, while the others decreased. The LPI showed an increase in the extremely low LST zones and decrease in the very high and extremely high LST zones. LSI decreased across all levels except very low and medium low LST zones, while AI decreased in these two zones. CONTAG generally decreased, while SHDI increased.

In Tieling, the total areas of extremely low and extremely high LST zones increased, while the others decreased. LPI rose in the very low and low LST zones, but declined in the extremely low and extremely high LST zones. LSI increased only in the extremely low and extremely high LST zones, while AI decreased solely in these zones. CONTAG generally decreased, while SHDI increased.

To further quantify the spatial pattern of SUHI, we analyzed the SUHI indicators from Section 2.4, with the results presented in Table 5. In Fushun, the overall MSU increased from 2000 to 2020. The SUR rose until 2014, followed by a decline. The SUSD followed a similar pattern, indicating that the standard deviations remained relatively stable across the four time periods. In Tieling, the total MSU showed a consistent upward trend. The total SUR increased until 2014, after which it declined. The SUSD increased slightly from 2000 to 2020, indicating that the standard deviations increased during the past 20 years.

3.2. Spatiotemporal evolution of land cover

Fig. 4. shows the land cover classification results. Comparing these results with the ΔLST map reveals a strong correlation between changes in IS and mining areas with areas of high SUHI. Therefore, we will further analyze the changes in land cover.

Tables A.2 and A.3 present the accuracy assessment results for land cover classification in Fushun and Tieling from 2000 to 2020. In Fushun, the overall classification accuracy for 2000, 2007, 2014 and 2020 was 93.72 %, 90.33 %, 91.72 % and 90.88 % with Kappa coefficients of 92.83 %, 87.76 %, 88.93 % and 88.54 %, respectively. In Tieling, the overall classification accuracy for 2000, 2006, 2014 and 2020 was 92.12 %, 91.44 %, 89.42 % and 90.33 %, with Kappa coefficients of 90.32 %, 90.08 %, 86.79 % and 88.74 %, respectively. These accuracy validation

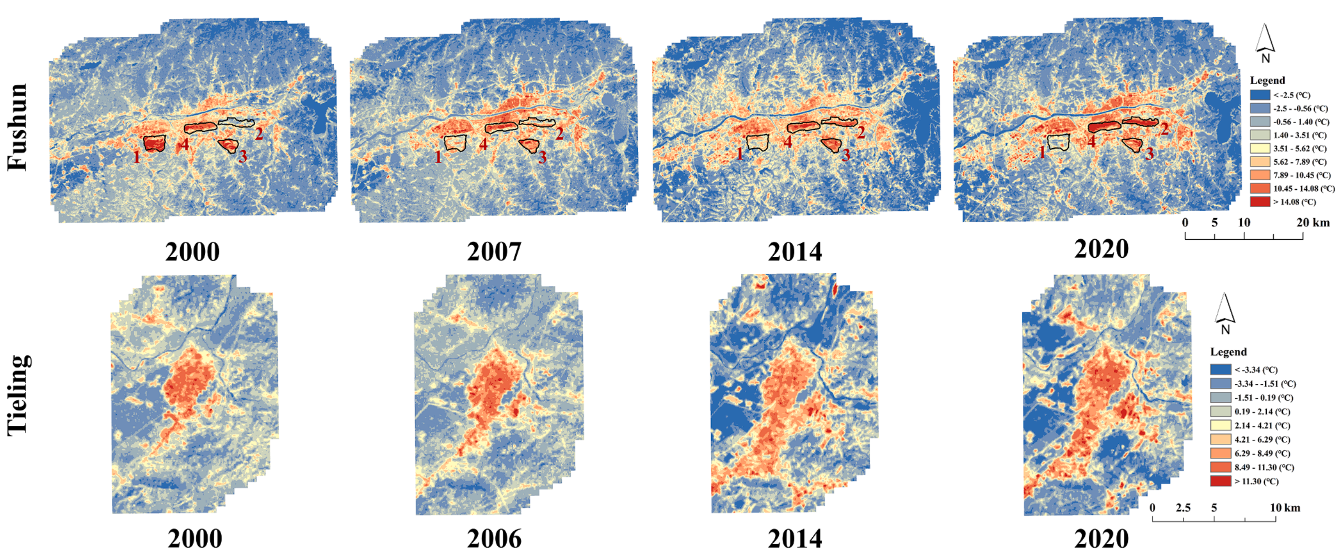

Fig. 3. The ΔLST map of Fushun and Tieling from 2000 - 2020. (1: West Dumping Site; 2: East Open-Pit; 3: East Dumping Site; 4: West Open-Pit).

Table 4
The slope of landscape pattern changes of LST levels from 2000 to 2020.

Fushun	PLAND	LPI	LSI	AI	CONTAG	SHDI
Extremely low	0.8717	1.2236	−1.5804	2.2030	−0.9812	0.0355
Very low	0.5030	−0.0273	2.8940	−3.6603		
Low	−0.2407	−0.0112	−2.1629	0.9133		
Medium low	0.3797	0.0010	1.0786	−1.8547		
Medium high	−0.3857	−0.0118	−1.5332	2.4799		
High	0.2200	0.0010	−1.1687	1.4608		
Very high	−1.9150	−1.3397	−2.0916	1.1503		
Extremely high	−1.8360	−1.6440	−0.9590	0.9235		
Tieling						
Extremely low	1.9882	−0.6936	1.4622	−0.7424	−0.9698	0.0839
Very low	−1.0370	2.0153	−3.5599	1.4818		
Low	−0.9414	1.0251	−3.3360	2.4747		
Medium low	−0.8157	−0.0025	−3.3801	1.0433		
Medium high	−0.7015	0.0002	−2.3599	2.4129		
High	−0.4474	−0.0029	−2.5877	1.9304		
Very high	−0.2960	0.0008	−0.1344	3.8996		
Extremely high	2.4455	−1.5335	1.3647	−0.6871		

Note: PLAND: Percentage of Landscape; PD: Patch Density; LPI: Largest Patch Index; LSI: Landscape Shape Index; AI: Aggregation Index; CONTAG: Contagion index; SHDI: Shannon's Diversity Index.

Table 5
The result of SUHI indicators in Fushun and Tieling from 2000 to 2020.

Fushun	**2000**	**2007**	**2014**	**2020**
MSU (unit: °C)	0.7685	0.8934	0.9444	1.0268
SUR (%)	25.19	26.13	34.02	31.19
SUSD (unit: °C)	3.2303	3.2728	3.7826	3.9039
Tieling	**2000**	**2006**	**2014**	**2020**
MSU (unit: °C)	0.6685	0.7416	0.7708	0.8556
SUR (%)	22.39	22.00	33.44	31.50
SUSD (unit: °C)	2.8098	2.8467	3.9218	3.9493

Note: MSU: mean SUHI; SUR: SUHI ratio; SUSD: SUHI standard deviation.

results confirm that the classification outcomes for each year in both study areas meet the required standards and are suitable for further research and analysis.

The land cover transitions in Fushun are shown in Fig. 5. (1) From 2000 to 2007, the most significant changes were the conversion of 40.67 km^2 of cropland to IS, 19.3 km^2 of forest to cropland, and 16.93 km^2 of IS to cropland. (2) Between 2007 and 2014, there were 69.8 km^2 of cropland was converted to IS, 28.6 km^2 of IS to cropland, and 20.87 km^2 of forest to cropland. (3) From 2014 to 2020, key changes included 33.29 km^2 of IS converted to cropland, 27.08 km^2 of cropland to IS, and 25.2 km^2 of cropland to forest and grassland. (4) Over the entire period from 2000 to 2020, cropland areas initially decreased but rebounded by 2020, while forest areas consistently declined, and grassland and IS areas steadily increased. Meanwhile, the cropland, forest, and IS were continuously converting into one another.

The land cover transitions in Tieling are shown in Fig. 6. (1) From 2000 to 2006, the primary changes were the conversion of 6.15 km^2 of cropland to IS, and 3.72 km^2 of IS to cropland. (2) Between 2006 and 2014, 11.9 km^2 of cropland was converted to IS, while 3.83 km^2 of IS was converted to cropland. (3) From 2014 to 2020, 9.02 km^2 of cropland was converted to grassland, forest, and IS, and 4.67 km^2 of IS was converted to cropland. (4) Over the entire period from 2000 to 2020, the trends in Tieling remained relatively consistent: cropland areas gradually decreased, forest, grassland and water areas remained stable, and IS areas steadily increased.

3.3. *Impacts of landscape composition and configuration on surface urban heat island (SUHI)*

To identify the factors influencing SUHI across different land cover types, the study first assessed their linear correlation with ΔLST at various scales in both study areas. The determination coefficients (R^2)

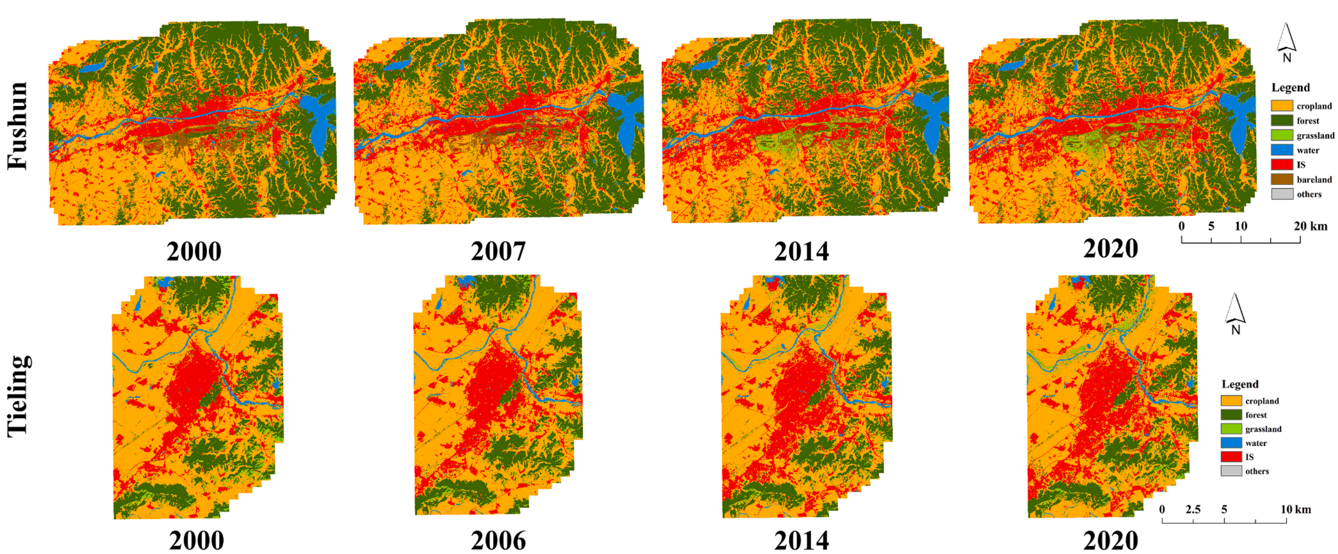

Fig. 4. The land cover map of Fushun and Tieling.

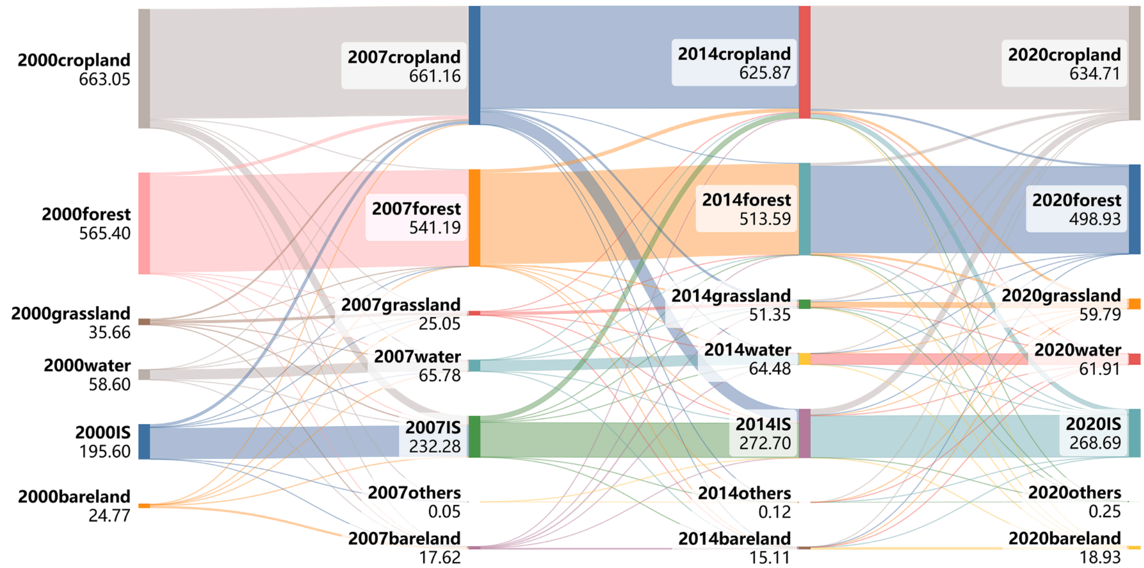

Fig. 5. Land cover transition over four periods in Fushun (in km^2).

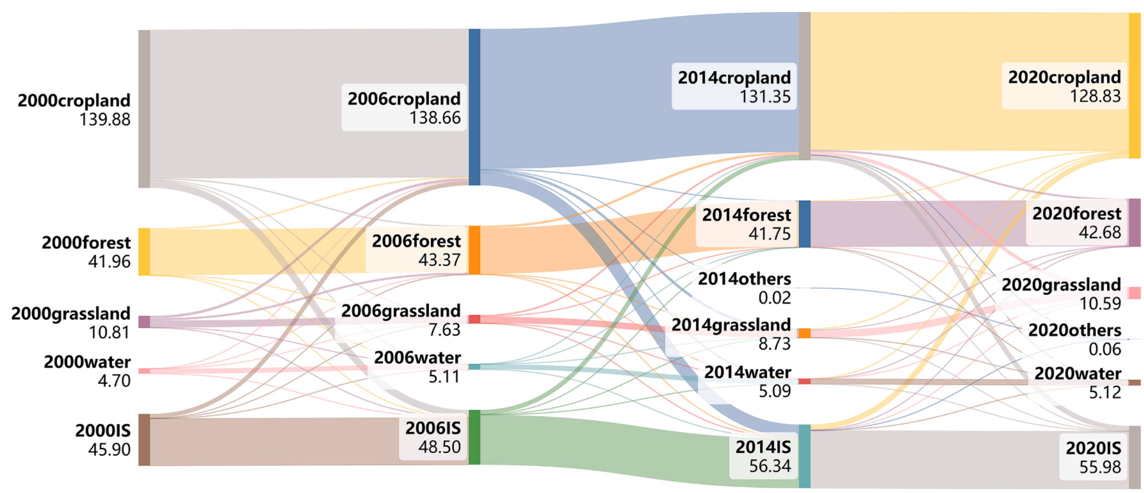

Fig. 6. Land cover transition over four periods in Tieling (in km^2).

are shown in **Tab. A.4**. The results show IS consistently exhibited a strong correlation with ΔLST across all grid sizes. The bare land in Fushun and the forest also showed significant correlations. However, due to the limited area of bare land, its inclusion in regression analysis would considerably reduce the available data. Therefore, only IS and forest were selected for further analyses.

Considering the geographic characteristics and location of the study, we opted for the MGWR regression method to better account for the inherent geographic correlations within the data. After collinearity test performed, the independent variables in this study included PLAND_forest, PD_forest, LSI_forest, AI_forest, PLAND_IS, PD_IS, LSI_IS, AI_IS, CONTAG, SHDI, and population, with ΔLST as the dependent variables. MGWR analysis was conducted separately for the two study areas at various grid scales. Since the population data was derived from the Landscan dataset with a spatial resolution of 1 km, it was excluded from the analysis at the grid scales of 300 m, 600 m, and 900 m. The MGWR analysis results are detailed in Table 6.

The models show high accuracy, with R^2 and Adjusted R^2 values exceeding 0.6 in all cases except for models at the 300 m scale in Fushun. However, it's important to consider the potential issue of overfitting due to the limited number of observations.

For Fushun City, PLAND_IS exhibited the strongest positive correlation, while PLAND_forest showed a negative correlation across all scales and years. (1) At 300 m scale, PD_IS showed a slight positive correlation. (2) At 600 m scale, LSI_forest in 2014 and SHDI in 2000 showed positive correlations. (3) At 900 m scale, LSI_forest in 2014 and SHDI in 2000 showed positive correlations. (4) At 1200 m scale, LSI_forest showed a slight positive correlation in 2014 and 2020. However, the population variable did not pass the significance test or had a weak correlation.

For Tieling City, PLAND_IS also exhibited the strongest positive correlation, while PLAND_forest showed a negative correlation across all scales and years. (1) At 300 m scale, LSI_forest showed a positive correlation in 2006, while LSI_IS showed a positive correlation in 2006 and 2014. (2) At 600 m scale, LSI_forest showed a slight positive correlation in 2000 and 2006. (3) At 900 m scale, PLAND_forest did not pass the significant test in 2014 and 2020. (4) At 1200 m scale, LSI_forest showed a positive correlation in 2000 and 2014. The population also did not pass the significance test or exhibited a weak correlated.

Table 6
The MGWR analysis results of ΔLST in Fushun and Tieling.

Fushun					Tieling			
300 m	**2000**	**2007**	**2014**	**2020**	**2000**	**2006**	**2014**	**2020**
Intercept	−0.040	−0.023	−0.000	−0.013	−0.105	−0.058	0.009	−0.029
PLAND_forest	−0.141**	−0.198**	−0.194**	−0.167**	−0.184**	−0.196**	−0.188**	−0.086
PD_forest	0.009**	−0.006	−0.018	−0.009*	0.012	0.010	0.001	0.028
LSI_forest	−0.033**	−0.004**	0.044**	0.000**	0.029	0.116**	0.028	0.106*
AI_forest	0.006	−0.016**	−0.021**	−0.011**	−0.007*	0.036	0.017*	0.069*
PLAND_IS	0.504**	0.491**	0.488**	0.571**	0.557**	0.693**	0.540**	0.728**
PD_IS	0.031**	0.029**	0.017**	0.033**	−0.044	0.024	0.031	0.059
LSI_IS	−0.029*	−0.005	0.016	−0.006	0.076	0.103*	0.106**	0.092*
AI_IS	−0.029*	−0.018	−0.015	−0.026**	0.011	−0.012	0.075	0.021
CONTAG	−0.084*	−0.018**	−0.072	−0.053**	–	–	–	–
SHDI	0.030	0.052**	0.020**	0.016	0.088	−0.024*	0.020	−0.040
R^2	0.575	0.664	0.591	0.673	0.606	0.716	0.609	0.686
AdjR^2	0.574	0.663	0.591	0.672	0.595	0.710	0.603	0.681
observations	3700	3933	4204	4663	337	431	548	546
600 m								
Intercept	−0.044	−0.019	−0.005	−0.038	−0.064	−0.042	0.062	0.014
PLAND_forest	−0.124**	−0.205**	−0.152**	−0.184**	−0.195**	−0.135**	−0.176**	−0.101**
PD_forest	−0.032**	−0.011	−0.024	0.007	−0.017	0.022	0.005	−0.028
LSI_forest	0.004**	0.033**	0.110**	0.037	0.118*	0.102**	0.063	0.069
AI_forest	−0.068*	−0.018*	−0.031	−0.017**	0.055**	0.025*	0.077**	0.028
PLAND_IS	0.585**	0.629**	0.636**	0.827**	0.738**	0.813**	0.642**	0.775**
PD_IS	0.077**	0.072**	0.031**	0.048**	0.009	0.068	0.015	0.017
LSI_IS	−0.06**	−0.040**	0.025	−0.035**	−0.041	0.019	0.050*	0.078*
AI_IS	−0.019	−0.023**	−0.006	−0.023**	−0.039	0.005	0.076	0.025
SHDI	0.134**	0.042**	0.032	0.053**	−0.022	−0.072*	−0.018	0.014
R^2	0.701	0.790	0.737	0.813	0.735	0.874	0.725	0.802
AdjR^2	0.699	0.789	0.736	0.813	0.726	0.870	0.717	0.796
observations	2146	2125	2256	2438	257	294	329	335
900 m								
Intercept	−0.034	−0.024	−0.005	−0.029	−0.058	−0.065	0.080	−0.002
PLAND_forest	−0.107**	−0.180**	−0.152**	−0.082**	−0.149**	−0.091**	−0.084	−0.054
PD_forest	−0.014**	−0.007	−0.024	0.011	0.030	0.041	0.062*	−0.002
LSI_forest	0.024**	0.060**	0.110**	0.077**	0.025	0.057**	−0.009	0.035
AI_forest	−0.073	−0.020	−0.031	−0.001	0.058**	0.063**	0.073**	0.001
PLAND_IS	0.641**	0.686**	0.636**	0.775**	0.843**	0.885**	0.762**	0.869**
PD_IS	0.083	0.061**	0.031**	0.056**	0.037	0.073*	−0.010	−0.025*
LSI_IS	−0.081	−0.015	0.025	0.002	−0.152	−0.010	0.055*	0.058
AI_IS	−0.018	−0.015	−0.006	−0.008	−0.090*	−0.027	−0.018	−0.030
SHDI	0.117	0.017	0.032	−0.005	0.081*	−0.073	0.037	0.092**
R^2	0.753	0.835	0.737	0.853	0.825	0.894	0.772	0.859
AdjR^2	0.751	0.833	0.736	0.852	0.815	0.889	0.762	0.853
observations	1275	1254	1314	1380	173	188	209	217
1200 m								
Intercept	−0.071	0.012	−0.036	−0.021	−0.040	−0.042	−0.018	−0.012
PLAND_forest	−0.120**	−0.157**	−0.061**	−0.039**	−0.242**	−0.155**	−0.139	−0.046
PD_forest	−0.057**	−0.019	0.025	−0.002	0.034	−0.018	0.008	−0.003
LSI_forest	0.095**	0.075**	0.113**	0.103**	0.168	0.099**	−0.008	0.110
AI_forest	−0.021	−0.055	−0.019	−0.004	0.167*	0.078**	0.136**	0.028
PLAND_IS	0.721**	0.681**	0.824**	0.838**	0.922**	0.978**	0.818**	0.915**
PD_IS	0.151	0.051**	0.087*	0.090**	−0.114	0.062	−0.075*	−0.073*
LSI_IS	−0.136	0.000	−0.027	−0.017	−0.083	−0.116	0.073*	0.079
AI_IS	−0.011	−0.021	−0.009	−0.012	−0.095	−0.073	0.007	−0.001
SHDI	0.110	0.014	0.038	−0.001*	0.010*	−0.022	0.110	0.048*
Population	−0.067*	0.073**	−0.067	0.015	0.067**	−0.002	−0.042*	0.077
R^2	0.782	0.880	0.834	0.871	0.876	0.926	0.848	0.877
AdjR^2	0.780	0.878	0.832	0.869	0.865	0.920	0.836	0.867
observations	869	829	863	894	118	132	138	138

Note:
* Sig. p-value < 0.05;.
** Sig. p-value < 0.01.

4. Discussion

4.1. *Spatiotemporal characteristic evolution of surface urban heat island (SUHI) in Fushun city*

The shrinking of Fushun is driven by the decline in labor demand and population outflow due to industrial upgrading (Zhang, 2022). Its SUHI patterns had become atypical due to changes in mining activity. Although the proportion of extremely high LST zones had decreased, these areas had become more spatially clustered, particularly in mining or central urban zones. This suggested a shift towards concentration rather than dispersion. Additionally, SUR peaked in 2014, closely linked to the resumption of the East Open Pit after 2004, signaling more frequent strong heat islands.

Fushun's spatiotemporal pattern of SUHI is closely linked to migration of mining areas (refer to Fig. 3 for the distribution of mining areas). There are four major mining areas in Fushun: (1) West Dumping Site (Fig. 3 Fushun part 1): Established in 1937 and closed in 2000 due to industrial restructuring (Zhang, 2022). Through continuous vegetation planting, the land cover transitioned from impervious surfaces to cropland and grassland, changing it from a heat island to a cold island over the past 20 years. (2) East Open-Pit (Fig. 3 Fushun part 2): Development resumed in 2004 after several mining stoppages (Zhang, 2022). The land cover changed from cropland and grassland to bare land and impervious surfaces. Since 2007, SUHI has intensified, gradually turning this area into a new high SUHI zone. (3) East Dumping Site (Fig. 3 Fushun part 3): Used for 20 years, with improved environmental awareness and resource allocation since the 21st century (FMDRC, 2022). The land cover shifted from impervious surfaces to grassland, resulting in a decrease in SUHI, demonstrating effective environmental efforts. (4) West Open-Pit (Fig. 3 Fushun part 4): As Asia's largest open-pit coal mine, it provided abundant resources but also presented significant risks of environmental pollution and geological disasters. Production gradually declined, and the mine was closed in 2019 (Feng & Xu, 2023). However, the SUHI change was not significant, indicating a need for further ecological restoration.

Why does mining areas, as permeable surfaces, having a strong correlation with SUHI? To explore this, we further investigated by analyzing the Normalized Difference Vegetation Index (NDVI) and Bare Soil Index (BSI) using MODIS datasets from four periods, characterizing changes in greenness and bare soil exposure within the mining areas (Fig. 7). The results show that as construction progressed in the mining areas (2: East Open-Pit), overall greenness continuously declined, while recovery (1: West Dumping Site) followed the opposite trend. Due to Fushun's open-pit coal mining, the surfaces of mining areas tend to be high-reflective bare soil, leading to higher LST compared to typical suburban surfaces.

Our study results show that IS has the most significant impact on increasing SUHI, while forest plays the most significant role in reducing SUHI, consistent with previous studies (Xu et al., 2024; Wu et al., 2022). In Fushun, PD_IS, LSI_forest, and SHDI demonstrated varying warming effects across different scales and years. The patch density of IS showed a correlation at small scales (300 m), while the landscape shape of forest exhibited correlation at larger scales (greater than 300 m). This suggests that minimizing the number of IS patches at smaller scales and maintaining forest integrity at larger scales can help mitigate the urban heat island effect to some extent. SHDI reflects land cover diversity, indicating that as urbanization progresses, the increasing variety of surface types intensifies SUHI.

4.2. Spatiotemporal characteristic evolution of surface urban heat island (SUHI) in Tieling city

Tieling does not have a dominant industrial sector, and its population has steadily declined over the years due to various factors (Yu et al., 2023). The LST patterns followed a more regular trend. The proportion of extremely high and extremely low LST zones increased, but the clustering of these zones decreased, indicating the expansion of IS and intensified land cover changes, similar to phenomena seen in urban expansion (Liang et al., 2021). The trends of CONTAG and SHDI were similar to Fushun, driven by subsurface conditions linked to the expansion of impervious surfaces. The SUHI in Tieling peaked in 2020, showing an increase trend.

So why does Tieling's SUHI resemble that of expanding cities, despite its declining population? This is related to the unique development pattern of shrinking cities in China, where population decline is accompanied by spatial expansion. Chinese planners and local authorities, focused on urbanization, often overlook issues like population loss and economic decline (Meng & Long, 2022). This growth-oriented paradigm ultimately leads to an oversupply of built-up areas in shrinking cities (Long & Gao, 2019), resulting in population loss alongside urban expansion. And this remains a key challenge for shrinking cities in China.

Based on the analysis of SUHI influencing factors, the results for Tieling and Fushun were consistent, both highlighting the critical role of IS and forest in regulating SUHI. Regarding the population factor, which this study focus on, some research suggests that the decline in anthropogenic heat due to a shrinking urban population affects SUHI (Mansour et al., 2022; Mohammad & Goswami, 2023; Wang et al., 2023c), while others find no significant correlation between the two (Liu & Zhang, 2024; Cai et al., 2021). Our findings indicate that the population factor does not significantly influence SUHI, consistent with previous studies. Therefore, this study further supports the argument that population factors have little to no impact on SUHI.

4.3. Comparison between Fushun and Tieling

In Fushun City, a typical coal-based shrinking city, the evolution of urban development and SUHI was closely tied to changes in the mining

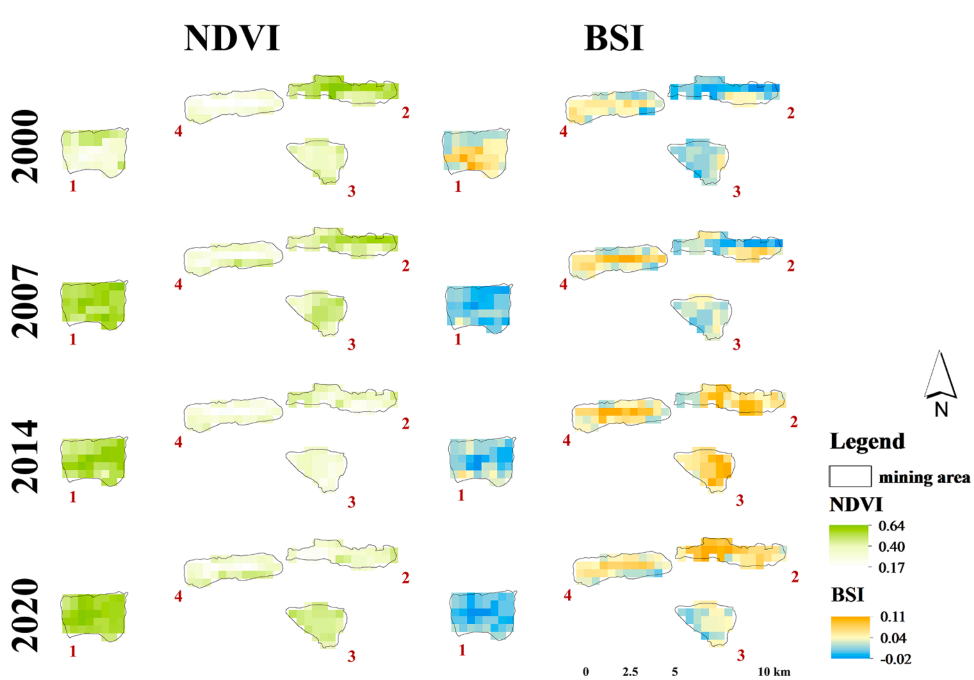

Fig. 7. NDVI and BSI change map for the mining areas. (1: West Dumping Site; 2: East Open-Pit; 3: East Dumping Site; 4: West Open-Pit).

areas. Despite population decline, the city's mining and industrial sectors continued to expand, making its urban contraction atypical due to the dominance of mining. The closure of the West Dumping Site had slightly improved the SUHI problem, but the reactivation of the East Open Pit near the city had introduced new challenges to its thermal environment. For sustainable development, Fushun should follow the example of the East Dumping Site revitalization by prioritizing green restoration alongside ongoing mining activities and implementing diverse vegetation initiatives to enhance the ecological landscape of mining areas (Xu & Cheng, 2024). Transitioning the coal industry, developing new energy sources, and promoting a circular urban economy could help Fushun mitigate the UHI effect while preserving its resources and environment.

Compared to Fushun, a shrinking city driven by the coal industry, Tieling represents a typical Chinese shrinking city characterized by population loss and spatial expansion. Our MGWR results showed that while the population factor was insignificant, and surface conditions continued to play a dominant role in shaping SUHI patterns, similar to those in expanding cities (Renc & Łupikasza, 2024). Planners and local authorities should promptly adjust urban development strategies and halt uncontrolled expansion. Efforts should shift from developing built-up areas to focusing on forests or natural parks, thereby enhancing biodiversity and improving the overall urban environment. Although shrinking cities are not inherently negative, they require careful management. Each region should adjust its development strategies based on local conditions and pursue sustainable growth.

4.4. Limitation and future perspectives

This study thoroughly analyzed and compared the spatiotemporal pattern evolution of SUHI in two types of shrinking cities, both affected by population loss and spatial expansion. However, the study has the following limitations:

(1) The analysis is limited by the availability of satellite image data, focusing on specific years within the 20-year period. Increasing data density by including additional years would strengthen the research methodology.
(2) Although the study focus on the spatiotemporal pattern of SUHI, the population data quality, derived from the Landscan dataset with a 1 km resolution, is limited. Using more precise population data at smaller scales could improve the accuracy of regressors and results.
(3) To better quantify the impact of population factors, future studies could explore multiple methods for assessing anthropogenic heat. However, when utilizing remote sensing data, it is crucial to consider imaging timing and short-term heat variations.

5. Conclusion

Through a 20-year analysis of the spatiotemporal pattern evolution of SUHI in Fushun and Tieling, both affected by population loss and urban expansion, we identified key changes in SUHI in shrinking cities and proposed methods to mitigate the UHI problem based on factors influencing SUHI. In Fushun, we found that SUHI in resource-based cities follows the migration of mining areas, with strong heat islands clustering in the mining areas and dispersed elsewhere. In Tieling, as urban areas expanded, SUHI intensified, and extremely high and extremely low LST zones became more dispersed. According to MGWR results, the percentage of impervious surfaces played a decisive role in SUHI in both cities, followed by the percentage of forest, with population factors having minimal impact. This study suggests that increasing the complexity and fragmentation of impervious surface (e.g., constructing landscapes with alternating vegetation, water, and impervious surfaces) could help mitigate SUHI in shrinking cities. This study offers insights for urban planning in shrinking cities to mitigate UHI and promote sustainable, livable communities.

CRediT authorship contribution statement

Yanfei Wu: Writing – review & editing, Writing – original draft, Visualization, Methodology, Investigation, Formal analysis, Data curation, Conceptualization. **Junjie Qiu:** Writing – review & editing, Validation. **Jiake Wang:** Writing – review & editing, Validation, Conceptualization. **Wenyuan Wu:** Writing – review & editing. **Ting Wu:** Writing – review & editing, Supervision. **Hao Hou:** Writing – review & editing. **Haiping Xia:** Writing – review & editing. **Junfeng Xu:** Writing – review & editing, Supervision, Methodology, Formal analysis, Conceptualization.

Declaration of competing interest

The authors declare that they have no known competing financial interests or personal relationships that could have appeared to influence the work reported in this paper.

Acknowledgment

This study was funded by the Natural Science Foundation of Zhejiang Province (grant number: LGF22D010008; Representative: Junfeng Xu). The conclusions and recommendations presented in this article are of the authors and do not, in any way, represent the views of the funder.

Supplementary materials

Supplementary material associated with this article can be found, in the online version, at doi:10.1016/j.scs.2024.105912.

Data availability

Data will be made available on request.

References

Aslam, R. W., Shu, H., & Yaseen, A. (2023). Monitoring the population change and urban growth of four major Pakistan cities through spatial analysis of open source data. *Annals of GIS, 29*(3), 355–367. https://doi.org/10.1080/19475683.2023.2166989
Cai, Z., Tang, Y., & Zhan, Q. (2021). A cooled city? Comparing human activity changes on the impact of urban thermal environment before and after city-wide lockdown. *Building and Environment, 195*, Article 107729. https://doi.org/10.1016/j.buildenv.2021.107729
Chauhan, S., & Singh Jethoo, A. (2023). Thermal characterization of Ajmer City: Insights into urban heat dynamics. *Materials Today: Proceedings*. https://doi.org/10.1016/j.matpr.2023.08.099. S2214785323043511.
Chen, D., Fang, C., & Liu, Z. (2023a). Progress and major themes of research on urban shrinkage and its eco-environmental impacts. *Journal of Geographical Sciences, 33*(5), 1113–1138. https://doi.org/10.1007/s11442-023-2122-x
Chen, L., Qi, Q., Wu, H., Feng, D., & Zhu, E. (2023b). Will the landscape composition and socio-economic development of coastal cities have an impact on the marine cooling effect? *Sustainable Cities and Society, 89*, Article 104328. https://doi.org/10.1016/j.scs.2022.104328
Chen, Y., Yang, J., Yu, W., Ren, J., Xiao, X., & Xia, J. C. (2023c). Relationship between urban spatial form and seasonal land surface temperature under different grid scales. *Sustainable Cities and Society, 89*(December 2022), Article 104374. https://doi.org/10.1016/j.scs.2022.104374
Cheng, J., Chen, M., & Tang, S. (2023). Shenzhen – A typical benchmark of Chinese rapid urbanization miracle. *Cities (London, England), 140*, Article 104421. https://doi.org/10.1016/j.cities.2023.104421
Cuypers, S., Nascetti, A., & Vergauwen, M. (2023). Land Use and Land Cover Mapping with VHR and Multi-Temporal Sentinel-2 Imagery. *Remote Sensing, 15*(10), 10. https://doi.org/10.3390/rs15102501
Dash, P., Sanders, S. L., Parajuli, P., & Ouyang, Y. (2023). Improving the Accuracy of Land Use and Land Cover Classification of Landsat Data in an Agricultural Watershed. *Remote Sensing, 15*(16), 16. https://doi.org/10.3390/rs15164020
Ding, W., & Liu, J. (2023). Nonlinear and spatial spillover effects of urbanization on air pollution and ecological resilience in the Yellow River Basin. *Environmental Science*

and Pollution Research, 30(15), 43229–43244. https://doi.org/10.1007/s11356-023-25193-4
Ellena, M., Melis, G., Zengarini, N., Di Gangi, E., Ricciardi, G., Mercogliano, P., & Costa, G. (2023). Micro-scale UHI risk assessment on the heat-health nexus within cities by looking at socio-economic factors and built environment characteristics: The Turin case study (Italy). *Urban Climate, 49*, Article 101514. https://doi.org/10.1016/j.uclim.2023.101514
Feng, D., & Xu, D. (2023). Research on the Beibang Geological Disaster Management and Building Reinforcement in the Influence Area in Fushun West Open-pit Mine. *China Academic Journal Electronic Publishing House, 43*(12), 64–68. https://doi.org/10.13626/j.cnki.hs.2023.12.008
FMDRC, F.M.D. and R C. (2022, September 30). *Make every effort to integrate and utilize this great article*. https://fsfgw.fushun.gov.cn/xwdt/001001/20220930/e064902d-192c-4bba-ab6a-a897dc515762.html.
Guan, S., Liu, S., Zhang, X., Du, X., Lv, Z., & Hu, H. (2023). Analysis of Supply–Demand Relationship of Cooling Capacity of Blue–Green Landscape under the Direction of Mitigating Urban Heat Island. *Sustainability, 15*(14), 14. https://doi.org/10.3390/su151410919
Han, D., Zhang, T., Qin, Y., Tan, Y., & Liu, J. (2023a). A comparative review on the mitigation strategies of urban heat island (UHI): A pathway for sustainable urban development. *Climate and Development, 15*(5), 379–403. https://doi.org/10.1080/17565529.2022.2092051
Han, S., Hou, H., Estoque, R. C., Zheng, Y., Shen, C., Murayama, Y., & Hu, T. (2023b). Seasonal effects of urban morphology on land surface temperature in a three-dimensional perspective: A case study in Hangzhou, China. *Building and Environment, 228*, Article 109913. https://doi.org/10.1016/j.buildenv.2022.109913
Jabbar, H. K., Hamoodi, M. N., & Al-Hameedawi, A. N (2023). Urban heat islands: A review of contributing factors, effects and data. *IOP Conference Series: Earth and Environmental Science, 1129*(1), Article 012038. https://doi.org/10.1088/1755-1315/1129/1/012038
Jallu, S. B., Shaik, R. U., Srivastav, R., & Pignatta, G. (2022). Assessing the effect of covid-19 lockdown on surface urban heat island for different land use /cover types using remote sensing. *Energy Nexus, 5*, Article 100056. https://doi.org/10.1016/j.nexus.2022.100056
Jang, G., & Kim, S. (2021). Are decline-oriented strategies thermally sustainable in shrinking cities? *Urban Climate, 39*, Article 100924. https://doi.org/10.1016/j.uclim.2021.100924
Jibitha, J. B., Achu, A. L., Joseph, S., Prasood, S. P., Thomas, J., & Selvakumar, S. (2024). Assessment of changes in land use /land cover and land surface temperature in a fast-growing urban agglomeration of Southern India. *Environment, Development and Sustainability*. https://doi.org/10.1007/s10668-024-04494-9
Jin, K., Wang, F., & Wang, S. (2020). Assessing the spatiotemporal variation in anthropogenic heat and its impact on the surface thermal environment over global land areas. *Sustainable Cities and Society, 63*, Article 102488. https://doi.org/10.1016/j.scs.2020.102488
Karunaratne, S., Athukorala, D., Murayama, Y., & Morimoto, T. (2022). Assessing Surface Urban Heat Island Related to Land Use/Land Cover Composition and Pattern in the Temperate Mountain Valley City of Kathmandu, Nepal. *Remote Sensing, 14*(16). https://doi.org/10.3390/rs14164047
Ke, X., Men, H., Zhou, T., Li, Z., & Zhu, F. (2021). Variance of the impact of urban green space on the urban heat island effect among different urban functional zones: A case study in Wuhan. *Urban Forestry & Urban Greening, 62*, Article 127159. https://doi.org/10.1016/j.ufug.2021.127159
Khavarian-Garmsir, A. R. (2023). A systematic review of shrinking cities literature: Lessons from the past and directions for the future. *International Planning Studies, 28*(3–4), 219–238. https://doi.org/10.1080/13563475.2023.2205030
Lee, J.-E., Park, Y., & Newman, G. D. (2023). Twenty years of research on shrinking cities: A focus on keywords and authors. *Landscape Research, 48*(7), 884–899. https://doi.org/10.1080/01426397.2023.2201492
Li, L., Zhan, W., Hu, L., Chakraborty, T., Wang, Z., Fu, P., & Wang, S. (2023a). Divergent urbanization-induced impacts on global surface urban heat island trends since 1980s. *Remote Sensing of Environment, 295*, Article 113650. https://doi.org/10.1016/j.rse.2023.113650
Li, W., An, M., Wu, H., An, H., Huang, J., & Khanal, R. (2023b). The local coupling and tele coupling of urbanization and ecological environment quality based on multisource remote sensing data. *Journal of Environmental Management, 327*, Article 116921. https://doi.org/10.1016/j.jenvman.2022.116921
Li, X., Yang, B., Liang, F., Zhang, H., Xu, Y., & Dong, Z. (2023c). Modeling urban canopy air temperature at city-block scale based on urban 3D morphology parameters– A study in Tianjin, North China. *Building and Environment, 230*, Article 110000. https://doi.org/10.1016/j.buildenv.2023.110000
Liang, X., Ji, X., Guo, N., & Meng, L. (2021). Assessment of urban heat islands for land use based on urban planning: A case study in the main urban area of Xuzhou City, China. *Environmental Earth Sciences, 80*(8), 308. https://doi.org/10.1007/s12665-021-09588-5
Lin, J., Wei, K., & Guan, Z. (2024). Exploring the connection between morphological characteristic of built-up areas and surface heat islands based on MSPA. *Urban Climate, 53*, Article 101764. https://doi.org/10.1016/j.uclim.2023.101764
Liu, L., & Zhang, W. (2024). Contrary to expectation: The surface urban heat island intensity is increasing in population shrinking region while decreasing in population growing region-A comparative analysis from China. *PLOS ONE, 19*(3), Article e0300635. https://doi.org/10.1371/journal.pone.0300635
Long, Y., & Gao, S. (2019). Shrinking cities in China: The overall profile and paradox in planning. In Y. Long, & S. Gao (Eds.), *Shrinking cities in china: The other facet of urbanization* (pp. 3–21). Springer. https://doi.org/10.1007/978-981-13-2646-2_1.
LPBS, (Liaoning Province Bureau of Statistics). (2020, December 22). *Liaoning Provincial Statistical Yearbook*. https://tjj.ln.gov.cn/tjj/tjsj/tjnj/lntjnj/index.shtml.
M, A., Ahmed, S. A., & N, H (2023). Land use and land cover classification using machine learning algorithms in google earth engine. *Earth Science Informatics, 16*(4), 3057–3073. https://doi.org/10.1007/s12145-023-01073-w
Ma, Y., Mamitimin, Y., Tiemuerbieke, B., Yimaer, R., Huang, M., Chen, H., & Guo, X. (2023). Spatiotemporal Characteristics and Influencing Factors of Urban Heat Island Based on Geographically Weighted Regression Model: A Case Study of Urumqi City. *Land, 12*(11), 11. https://doi.org/10.3390/land12112012
Manoli, G., Fatichi, S., Schläpfer, M., Yu, K., Crowther, T. W., Meili, N., & Bou-Zeid, E. (2019). Magnitude of urban heat islands largely explained by climate and population. *Nature, 573*(7772), 55–60. https://doi.org/10.1038/s41586-019-1512-9
Mansour, K., Aziz, M. A., Hashim, S., & Effat, H. (2022). Impact of anthropogenic activities on urban heat islands in major cities of El-Minya Governorate, Egypt. *The Egyptian Journal of Remote Sensing and Space Science, 25*(2), 609–620. https://doi.org/10.1016/j.ejrs.2022.03.014
Meng, X., & Long, Y. (2022). Shrinking cities in China: Evidence from the latest two population censuses 2010–2020. *Environment and Planning A: Economy and Space, 54*(3), 449–453. https://doi.org/10.1177/0308518X221076499
Moazzam, M. F. U., & Lee, B. G. (2024). Urbanization influenced SUHI Of 41 megacities of the world using big geospatial data assisted with google earth engine. *Sustainable Cities and Society, 101*, Article 105095. https://doi.org/10.1016/j.scs.2023.105095
Mohammad, P., & Goswami, A. (2023). Exploring different indicators for quantifying surface urban heat and cool island together: A case study over two metropolitan cities of India. *Environment, Development and Sustainability, 25*(10), 10857–10878. https://doi.org/10.1007/s10668-022-02509-x
Najafzadeh, F., Mohammadzadeh, A., Ghorbanian, A., & Jamali, S. (2021). Spatial and Temporal Analysis of Surface Urban Heat Island and Thermal Comfort Using Landsat Satellite Images between 1989 and 2019: A Case Study in Tehran. *Remote Sensing, 13*(21), 21. https://doi.org/10.3390/rs13214469
Oke, T. R. (1995). The Heat Island of the Urban Boundary Layer: Characteristics, Causes and Effects. In J. E. Cermak, A. G. Davenport, E. J. Plate, & D. X. Viegas (Eds.), *Wind climate in cities* (pp. 81–107). Netherlands: Springer. https://doi.org/10.1007/978-94-017-3686-2_5.
Oshan, T., Li, Z., Kang, W., Wolf, L., & Fotheringham, A. (2019). mgwr: A Python Implementation of Multiscale Geographically Weighted Regression for Investigating Process Spatial Heterogeneity and Scale. *ISPRS International Journal of Geo-Information, 8*(6), 269. https://doi.org/10.3390/ijgi8060269
Pan, L., Yang, C., Han, J., Yan, F., Ju, A., & Kui, T. (2024). Comparing the Evolution of Land Surface Temperature and Driving Factors between Three Different Urban Agglomerations in China. *Sustainability, 16*(2), 2. https://doi.org/10.3390/su16020486
Pena Acosta, M., Dikkers, M., Vahdatikhaki, F., Santos, J., & Dorée, A. G. (2023). A comprehensive generalizability assessment of data-driven Urban Heat Island (UHI) models. *Sustainable Cities and Society, 96*, Article 104701. https://doi.org/10.1016/j.scs.2023.104701
Peng, W. (2022). Surface and canopy urban heat islands: Does urban morphology result in the spatiotemporal differences? *Urban Climate, 42*, Article 101136. https://doi.org/10.1016/j.uclim.2022.101136
Peng, X., Zhou, Y., Fu, X., & Xu, J. (2022). Study on the spatial-temporal pattern and evolution of surface urban heat island in 180 shrinking cities in China. *Sustainable Cities and Society, 84*, Article 104018. https://doi.org/10.1016/j.scs.2022.104018
Reed, K., & Sun, F. (2023). Investigating the potential for cool roofs to mitigate urban heat in the Kansas City metropolitan area. *Climate Dynamics, 60*(1–2), 461–475. https://doi.org/10.1007/s00382-022-06296-z
Renc, A., & Łupikasza, E. (2024). Changes in the surface urban heat island between 1986 and 2021 in the polycentric Górnośląsko-Zagłębiowska Metropolis, southern Poland. *Building and Environment, 247*, Article 110997. https://doi.org/10.1016/j.buildenv.2023.110997
Rodriguez-Galiano, V. F., Ghimire, B., Rogan, J., Chica-Olmo, M., & Rigol-Sanchez, J. P (2012). An assessment of the effectiveness of a random forest classifier for land-cover classification. *ISPRS Journal of Photogrammetry and Remote Sensing, 67*, 93–104. https://doi.org/10.1016/j.isprsjprs.2011.11.002
Sima, L., Liu, Y., Zhang, J., & Shang, X. (2024). Research on Summer Hourly Climate-Influencing Factors in Suburban Areas of Cities in CFA Zone—Taking Chengdu, China as an Example. *Buildings, 14*(10), 3083. https://doi.org/10.3390/buildings14103083
Shao, L., Liao, W., Li, P., Luo, M., Xiong, X., & Liu, X. (2023). Drivers of global surface urban heat islands: Surface property, climate background, and 2D/3D urban morphologies. *Building and Environment, 242*, Article 110581. https://doi.org/10.1016/j.buildenv.2023.110581
Shen, Z., Xu, X., Sun, Z., Jiang, Y., & Shi, H. (2023). Regional thermal environments (RTEs) and driving forces in six urban agglomerations of China and America. *Building and Environment, 235*, Article 110185. https://doi.org/10.1016/j.buildenv.2023.110185
Sun, H., Zhou, G., Liu, Y., Fu, H., & Jin, Y. (2024). Housing vacancy identification in shrinking cities based on multi-source data: A case study of Fushun city in Northeast China. *Journal of Geographical Sciences, 34*(1), 89–111. https://doi.org/10.1007/s11442-024-2196-0
Sun, J., & Zhou, T. (2022). Reconsidering the effects of urban form on PM2.5 concentrations: An urban shrinkage perspective. *Environmental Science and Pollution Research, 30*(13), 38550–38565. https://doi.org/10.1007/s11356-022-25044-8
Voogt, J. A., & Oke, T. R. (2003). Thermal remote sensing of urban climates. *Remote Sensing of Environment, 86*, 370–384. https://doi.org/10.1016/S0034-4257(03)00079-8

Wang, J., Zhou, W., & Zhao, W. (2023a). Higher UHI Intensity, Higher Urban Temperature? A Synthetical Analysis of Urban Heat Environment in Urban Megaregion. *Remote Sensing, 15*(24), 24. https://doi.org/10.3390/rs15245696

Wang, N., Chen, J., He, T., Xu, X., Liu, L., Sun, Z., & Han, D. (2023b). Understanding the differences in the effect of urbanization on land surface temperature and air temperature in China: Insights from heatwave and non-heatwave conditions. *Environmental Research Letters, 18*(10), Article 104038. https://doi.org/10.1088/1748-9326/acfc58

Wang, Q., Wang, X., Meng, Y., Zhou, Y., & Wang, H. (2023c). Exploring the impact of urban features on the spatial variation of land surface temperature within the diurnal cycle. *Sustainable Cities and Society, 91*, Article 104432. https://doi.org/10.1016/j.scs.2023.104432

Wang, Y., Zhang, Y., & Ding, N. (2023d). Regulatory Effect Evaluation of Warming and Cooling Factors on Urban Land Surface Temperature Based on Multi-Source Satellite Data. *Remote Sensing, 15*(20), 20. https://doi.org/10.3390/rs15205025

Wei, L., Wang, F., Tolomei, C., Liu, S., Bignami, C., Li, B., & Pan, X. (2023). Displacements of Fushun west opencast coal mine revealed by multi-temporal InSAR technology. *Geo-Spatial Information Science*, 1–17. https://doi.org/10.1080/10095020.2023.2239285

Weng, Q., Lu, D., & Schubring, J. (2004). Estimation of land surface temperature–vegetation abundance relationship for urban heat island studies. *Remote Sensing of Environment, 89*(4), 467–483. https://doi.org/10.1016/j.rse.2003.11.005

Wu, K., & Yao, C. (2021). Exploring the association between shrinking cities and the loss of external investment: An intercity network analysis. *Cities (London, England), 119*, Article 103351. https://doi.org/10.1016/j.cities.2021.103351

Wu, Y., Hou, H., Wang, R., Murayama, Y., Wang, L., & Hu, T. (2022). Effects of landscape patterns on the morphological evolution of surface urban heat island in Hangzhou during 2000 –2020. *Sustainable Cities and Society, 79*, Article 103717. https://doi.org/10.1016/j.scs.2022.103717

Xu, D., Wang, Y., Zhou, D., Wang, Y., Zhang, Q., & Yang, Y. (2024). Influences of urban spatial factors on surface urban heat island effect and its spatial heterogeneity: A case study of Xi'an. *Building and Environment, 248*, Article 111072. https://doi.org/10.1016/j.buildenv.2023.111072

Xu, H., & Cheng, W. (2024). Landscape Analysis and Ecological Risk Assessment during 1995–2020 Based on Land Utilization /Land Coverage (LULC) and Random Forest: A Case Study of the Fushun Open-Pit Coal Area in Liaoning, China. *Sustainability, 16*(6), 6. https://doi.org/10.3390/su16062442

Xu, S., & Zhang, D. (2024). Study of Urban Shrinkage and Population Index Coupling in Liaoning Province. In *Proceedings of the 2023 4th International Conference on Computer Science and Management Technology* (pp. 956–961). https://doi.org/10.1145/3644523.3644695

Yagoub, M. M., Tesfaldet, Y. T., AlSumaiti, T., Al Hosani, N., & Elmubarak, M. G (2024). Estimating population density using open-access satellite images and geographic information system: Case of Al Ain city, UAE. *Remote Sensing Applications: Society and Environment, 33*, Article 101122. https://doi.org/10.1016/j.rsase.2023.101122

Yang, M., Ren, C., Wang, H., Wang, J., Feng, Z., Kumar, P., & Cao, S.-J. (2024). Mitigating urban heat island through neighboring rural land cover. *Nature Cities*. https://doi.org/10.1038/s44284-024-00091-z

Yu, H., Fotheringham, A. S., Li, Z., Oshan, T., Kang, W., & Wolf, L. J. (2020). Inference in Multiscale Geographically Weighted Regression. *Geographical Analysis, 52*(1), 87–106. https://doi.org/10.1111/gean.12189

Yu, S., Wang, R., Zhang, X., Miao, Y., & Wang, C. (2023). Spatiotemporal Evolution of Urban Shrinkage and Its Impact on Urban Resilience in Three Provinces of Northeast China. *Land, 12*(7), 7. https://doi.org/10.3390/land12071412

Yue, X., Liu, W., Wang, X., Yang, J., Lan, Y., Zhu, Z., & Yao, X. (2024). Constructing an urban heat network to mitigate the urban heat island effect from a connectivity perspective. *Sustainable Cities and Society, 114*, Article 105774. https://doi.org/10.1016/j.scs.2024.105774

Zeng, T., Jin, H., Geng, Z., Kang, Z., & Zhang, Z. (2022). The Effect of Urban Shrinkage on Carbon Dioxide Emissions Efficiency in Northeast China. *International Journal of Environmental Research and Public Health, 19*(9), 5772. https://doi.org/10.3390/ijerph19095772

Zeng, P., Zong, C., Duan, Z., & Wei, X. (2023). Exploring the spatial interplay between built-up environments and surface urban heat island phenomena in the main urban area of Shanghai. *Energy and Buildings, 301*, Article 113739. https://doi.org/10.1016/j.enbuild.2023.113739

Zhang, B. (2022a). Prospect of intelligent mine construction in Fushun East Open-pit Mine. *Opencast Mining Technology, 37*(3), 107–109. https://doi.org/10.13235/j.cnki.ltcm.2022.03.027. +113.

Zhang, N., Zhang, J., Chen, W., & Su, J. (2022). Block-based variations in the impact of characteristics of urban functional zones on the urban heat island effect: A case study of Beijing. *Sustainable Cities and Society, 76*(August 2021), Article 103529. https://doi.org/10.1016/j.scs.2021.103529

Zhu, R., Dong, X., & Wong, M. S. (2022). Estimation of the urban heat island effect in a reformed urban district: A scenario-based study in Hong Kong. *Sustainability (Switzerland), 14*(8). https://doi.org/10.3390/su14084409